

# Reduced order modeling of two-link flexible manipulators using finite element modal decomposition

M. Sayahkarajy, E. Supriyanto, and Z. Mohamed

**Abstract**— This paper presents dynamic modelling of a two-link planar manipulator with flexible links, using a high order Finite Element (FE) model. First, using sufficiently high number of Euler-Bernoulli beam elements a high order model is derived for the multibody flexible system. The sufficiency of the number of elements is determined based on convergence of the FE model. The global vibration modes of the manipulator are derived from the global mass and stiffness matrices of the system. The gap between the complexity of high order FE models capable of predicting dynamic behavior of a flexible manipulator, and suitability of the FE model for controller design is bridged by a reduced order control scheme based on modal truncation/ $H_\infty$  techniques.

**Keywords**— Large scale systems, Elastic manipulators, Finite element modeling, Modal order reduction.

## I. INTRODUCTION

**F**LEXIBLE Manipulators (FMs) are known as the robotic arms designed with long and slender links in order to reduce their weight. As a more technical definition, the FM addresses a manipulator that its first structural natural frequencies are close to the operating speeds. This can happen due to either high acceleration motions, or low stiffness of the structure of the robot. Examples are the shuttle remote manipulator CANADARM [1], and high-speed industrial manipulators. The structural flexibility can happen due to elastic deflections of the links and/or joints. When the elastic deflections of the links of a manipulator are considered, the robot is known as “flexible link manipulator”. In the theory of elasticity, a flexible link is an infinite dimensional continuous system. For controller design and simulation, generally, a discrete finite dimensional model of such systems is required.

A widely used method of discretization of the governing equations of the FMs is the Assumed Mode Method (AMM). In AMM, [2],[3], vibration of each link is assumed to be

similar to the first vibration mode(s) of the link as a separate beam under some assumed Boundary Conditions (BC). The problem with the AMM, in particular in the case of multi-link manipulators, is that the vibration modes of a beam are very sensitive to the changes in the BCs, and so, describing the BCs of a moving link by classic BCs such as clamped, free, or carrying a mass/inertia can be a source of error. An alternative method that can provide a finite dimension model of a flexible multibody system is the method of Finite Elements (FE). The FE analysis has been used for open-loop or closed-loop simulation of the FMs by some researchers. Linear FE modelling and simulation of two-link FM is presented in [4], and [5]. Theoretical and experimental comparison of some modeling methods for FMs including AMM and FE model are presented in [6]. The potential advantage of FE is that the mode presumptions of AMM can be alleviated by using FE method. However, for good accuracy of dynamic analysis problems, FE normally requires the mechanical part be divided into high numbers of elements. It is a well-known fact in the field of FE analysis that a model meshed by  $n$  elements (e.g. divided into  $n$  elements) cannot predict “all” the  $n$  natural frequencies precisely. On the other hand, the high order models resulted from fine FE meshes can be too big for controller design algorithms. Therefore the researchers who used FE for a model based control design have had a tendency to use just one or two elements to model each link, ignoring any analysis addressing sufficiency of the low number of elements for modeling the FMs. The potential of multi-element FE models for model-based controller design has been shown in [7] and [8].

In this work, an FE model is established using the Euler-Bernoulli beam elements and lumped mass model with arbitrary number of elements. The governing equations of motion are derived using the Lagrange’s equations. Then an analysis of the linearized FE model is presented to show incapability of the FE models having low number of elements in modeling the system in terms of repeatability, on one hand, as well as the independency of the model to the number of elements when the number of elements is chosen sufficiently high (here around 50 elements for each link). The high order FE model satisfying the convergence is then verified by some measures including the FE software “Abaqus CAE”. In order to prepare the model for a model based control algorithm, the FE model is approximated to a low order system by

M. Sayahkarajy is a researcher of Universiti Teknologi Malaysia under the post-doctoral fellowship scheme for the project: “Optimization of TEE Echocardiography” (e-mail: sayahkarajy@gmail.com).

Z. Mohamed is with the Faculty of Electrical Engineering, Universiti Teknologi Malaysia, 81310, Johor Bahru Malaysia (e-mail: zahar@fke.utm.my).

E. Supriyanto is with the Advanced Diagnostics and Progressive Human Care Research Group, IJN-UTM Cardiovascular Engineering Centre, Faculty of Biosciences and Medical Engineering, Universiti Teknologi Malaysia, 81310, Johor Bahru Malaysia (corresponding author Phone: +60-16 776 30 04 e-mail: eko@utm.my).

employing modal decomposition and model reduction. In this manner the resultant dynamic equations preserve the precision of a finely meshed FE model in low frequencies of interest or bandwidth of the system, while the order of the system is not too big for control algorithms.

One importance of the proposed model is that it is free of the assumptions of Component Modes Analysis and the Floating Frame of References that are used in the field of Flexible Multibody Dynamics; and so, predicts the global vibration modes of the system. Another advantage is that the real power of FE is employed when sufficiently high numbers of elements are used.

II. THE PHYSICAL MODEL ELEMENTS

An isometric drawing of a typical two-link manipulator is depicted in Figure 1. The first link has a rotational degree of freedom (DOF) around the axis of joint “1” with respect to the ground and is driven by DC motor “1”. On the axis of joint “2”, the links are connected (hinged) to each other through the shaft of DC motor “2”. The manipulator is supposed to maneuver in a horizontal plane. Additionally, due to the thin rectangular cross-sections, the links have small in-plane elastic bending.

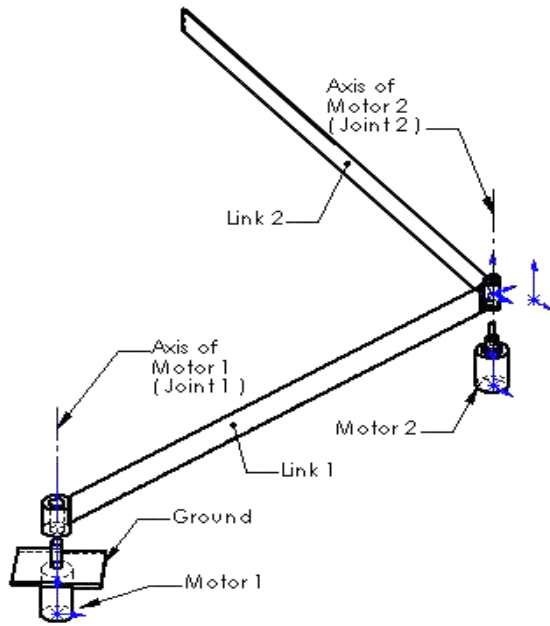


Fig. 1 A Typical Two-Link Flexible Manipulator.

Table 1 shows the system parameters used for simulation. The inputs of the system are the torques applied by the motors on the joints. The measured parameters or the outputs of the system are the angular position of the links described by the joint angles, and position of the tip or the end effector of the robotic arm.

To derive the dynamic equations of the system, an FE discretization is used for the two-link FM. Each link is modeled with a finite number of Euler-Bernoulli beam elements, incorporating the mass of each element as two lumped masses at the tips of the element. Figure 2(a) shows a

prototype beam element of the system with two nodes A and B. The straight line AB shows the neutral axis of the undeformed element. Each node “i” has two DOF that is described by two independent variables  $u_i$  the linear displacement, and  $\varphi_i$  the rotation of the node. The lumped mass assumption will result in a “diagonal” mass matrix for the FE model of the system; which simplifies numerical measurements. A meshed model under exaggerated deformations is shown in Figure 2(b). The unknowns of the dynamic equation consist of a vector of “n” independent coordinates including  $u_{i,j}, \varphi_{i,j}$ , the linear and angular displacements of each node  $i$  of link  $j=1,2$  as

$$\bar{q} = \{q_1, q_2, q_3, \dots, q_n\}^T =$$

$$(q_1 = u_{1,1}, \quad q_2 = \varphi_{1,1}, \quad q_3 = u_{2,1}, \quad \dots, \quad q_n = \varphi_{N,2}) \tag{1}$$

where  $N$  is the number of nodes used for meshing each link; and  $n=4N$  is the (minimum) number of generalized coordinates. The superscript  $T$  stands for “Transpose” in this paper. The partitioning line in (1) separates the nodal coordinates of the first and the second links.

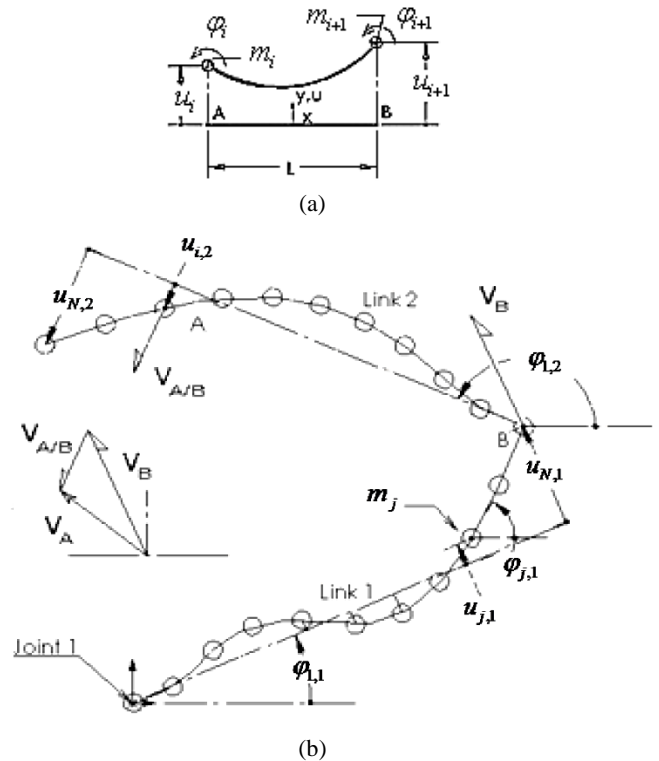


Fig.2 FE discretization: (a) a two-node Euler-Bernoulli beam element; (b) The meshed FE model

III. DYNAMIC EQUATIONS

A. Formulation of the governing equations

For any structural system, the equations of motion can be obtained from the energy functions of the system. Hamilton’s principle that has a root in the principle of virtual displacements along with d’Alembert’s principle presents the

integral form of the governing equations of motion. For the holonomic  $n$  DOF discrete system, Hamilton's principle takes a more convenient form known as Lagrange's equations. As the manipulator moves in a horizontal plane, the effects of gravity is ignored, and so, the only type of potential energy present here is the elastic potential energy or strain energy  $U$ . The Lagrangian  $L$  is derived from the overall kinetic energy  $T$  and the strain energy  $U$  by

$$L=T-U \quad (2)$$

The Lagrange's equations represent the relation between  $k=1,2,3,\dots,n$  generalized coordinates  $q_k$  and the generalized forces  $Q_k$ .

$$\frac{d}{dt} \left( \frac{\partial L}{\partial \dot{q}_k} \right) + \frac{\partial D}{\partial \dot{q}_k} - \frac{\partial L}{\partial q_k} = Q_k \quad (3)$$

The energy dissipation function due to damping shown by  $D$  in (3) is ignored at this stage; but damping effects will be taken into account by adding a modal damping coefficient  $\zeta$  in the modal coordinates. The generalized forces  $Q_k$  are related to the virtual work done by non-conservative forces which in turn can be related to the torques applied by the first and the second motors ( $\bar{\tau}_1, \bar{\tau}_2$ ) with the "n by 2" matrix  $F$  known as the input matrix given by

$$\sum_{k=1}^n Q_k \cdot \delta q_k = \delta W_{nc} = \sum_{k=1}^n (F_{k1} \bar{\tau}_1 + F_{k2} \bar{\tau}_2) \cdot \delta q_k \quad (4)$$

The energy of the system can be represented in a matrix form by defining "n by n" symmetric matrices  $M$  and  $K$  respectively known as the inertia and stiffness matrices as the following relations.

$$T = \frac{1}{2} \dot{\bar{q}}^T M \dot{\bar{q}} \quad ; \quad U = \frac{1}{2} \bar{q}^T K \bar{q} \quad (5)$$

Using these relations, the left hand side of (3) can be expressed as

$$\begin{aligned} & \frac{d}{dt} \left( \frac{\partial L}{\partial \dot{q}_k} \right) - \frac{\partial L}{\partial q_k} = \\ & \sum_j M_{kj} \ddot{q}_j + \sum_{i,j} \frac{\partial M_{kj}}{\partial q_i} \dot{q}_i \dot{q}_j - \frac{1}{2} \sum_{i,j} \frac{\partial M_{ij}}{\partial q_k} \dot{q}_i \dot{q}_j + \sum_j K_{kj} q_j \end{aligned} \quad (6)$$

The terms that include  $\dot{q}_i \dot{q}_j$  are the Coriolis and centripetal forces, and can be collected in a matrix  $C$  given by

$$C = [C_{kj}]; \quad C_{kj} = \frac{1}{2} \sum_i \left\{ \frac{\partial M_{kj}}{\partial q_i} + \frac{\partial M_{ki}}{\partial q_j} - \frac{\partial M_{ij}}{\partial q_k} \right\} \dot{q}_i \quad (7)$$

Then substituting equations, (4), (6), and (7) into (3) results in

$$M(\bar{q}) \ddot{\bar{q}} + K \bar{q} = F \{ \bar{\tau}_1, \bar{\tau}_2 \}^T - C(\bar{q}, \dot{\bar{q}}) \dot{\bar{q}}$$

It is supposed that the non-linear term  $C(\bar{q}, \dot{\bar{q}}) \dot{\bar{q}}$  is eliminated by a feed-forward input  $\{ \tau_{1C}, \tau_{2C} \}^T$  measured based on the dynamics of the equivalent rigid manipulator (see for example) so that  $F \{ \tau_{1C}, \tau_{2C} \}^T \approx C(\bar{q}, \dot{\bar{q}}) \Big|_{Rigid} \dot{\bar{q}}$ . Then using a change of variables  $\{ \bar{\tau}_1, \bar{\tau}_2 \}^T = \{ \tau_{1C}, \tau_{2C} \}^T + \{ \tau_1, \tau_2 \}^T$ , the matrix form of the equations of motion is given as follow

$$M(\bar{q}) \ddot{\bar{q}} + K \bar{q} = F \{ \tau_1, \tau_2 \}^T \quad (8)$$

To determine the matrix coefficients  $M$  and  $K$ , known as the global mass and stiffness matrices of the system, the energy expressions are obtained in matrix form. The kinetic and potential energies of the multi-DOF system can be described by  $n=4N$  independent nodal displacements that is shown as the vector of generalized coordinates  $\bar{q}$  in (1) and generalized velocities  $\dot{\bar{q}}$  as

$$\begin{aligned} \dot{\bar{q}} = & \\ & \{ \dot{u}_{1,1}, \dot{\phi}_{1,1}, \dot{u}_{2,1}, \dot{\phi}_{2,1}, \dots, \dot{u}_{N,1}, \dot{\phi}_{N,1} \mid \dot{u}_{1,2}, \dot{\phi}_{1,2}, \dots, \dot{u}_{N,2}, \dot{\phi}_{N,2} \}^T \end{aligned} \quad (9)$$

The overall energy expressions are measured by a superposition of the energies stored in the elements. The kinetic and potential energies of elements are measured for each of the links to find the global mass and stiffness matrices, in the next sections. For an arbitrary node "j" located on the first link (Figure 2(b)), kinematic relations of the velocity vector states that, under small elastic deflections  $u_{j,1}$ , the absolute value of velocity  $\bar{v}_j$  is given as

$$\left| \bar{v}_j \right| = (x_j \dot{\phi}_{1,1} + \dot{u}_{j,1}) \quad (10)$$

where  $\dot{\phi}_{1,1}$  is the angular velocity of the first motor, and  $x_j$  is the distance of point "j" from axis of joint "I". The kinetic energy carried by a concentrated mass  $m_j$  attached to point "j" then, can be given by

$$T_i = \frac{1}{2} m_j \bar{v}_j \cdot \bar{v}_j = \frac{1}{2} m_j \left| \bar{v}_j \right|^2 \quad (11)$$

Thus the kinetic energy of the first link is achieved by a summation of the kinetic energies of all of the  $N$  nodes as

$$T^{Link1} = \frac{1}{2} \sum_{j=1}^N \{m_j(x_j)^2 (\dot{\varphi}_{1,1})^2 + 2m_j x_j \dot{\varphi}_{1,1} \dot{u}_{j,1} + m_j (\dot{u}_{j,1})^2\} \quad (12)$$

The kinetic energy of the second link is also measured by the summation of the kinetic energy of its lumped masses. For an arbitrary node “ $i$ ” on the link 2, that is noted by point “ $A$ ” on Figure 2(b), the velocity vector  $\vec{v}_A$  can be represented by a vector summation of  $\vec{v}_B$  the velocity of point  $B$  (axis of joint 2), and  $\vec{v}_{A/B}$  the relative velocity of point  $A$  with respect to  $B$ . The kinematic relativity rule is

$$\vec{v}_A = \vec{v}_B + \vec{v}_{A/B}, \quad (13)$$

$\vec{v}_B$  and  $\vec{v}_{A/B}$  are respectively perpendicular to the first and the second link. The velocity vector of point  $B$  can be written as

$$\vec{v}_B = (l\dot{\varphi}_{1,1} + \dot{u}_{N,1}) \{-\sin \varphi_{1,1}, \cos \varphi_{1,1}\}^T \quad (14)$$

where  $\dot{u}_{N,1}$  represents the time derivative of the deflection of point  $B$  (the tip of the first link), and  $l$  is the distance of  $B$  from  $O$  (the axis of joint “ $1$ ”). The relative velocity of  $A$  is given by

$$\vec{v}_{A/B} = (x_i \dot{\varphi}_{1,2} + \dot{u}_{i,2}) \{-\sin \varphi_{1,2}, \cos \varphi_{1,2}\}^T \quad (15)$$

where  $\dot{\varphi}_{1,2}$  is the angular velocity of the second link,  $x_i$  is the distance of  $A$  from  $B$ , and  $\dot{u}_{i,2}$  represents the time derivative of the deflection of point  $A$ . Then the global velocity of the arbitrary point  $A$  can be obtained as

$$\vec{v}_A = \{-(l\dot{\varphi}_{1,1} + \dot{u}_{N,1}) \sin \varphi_{1,1} - (x_i \dot{\varphi}_{1,2} + \dot{u}_{i,2}) \sin \varphi_{1,2}, \\ (l\dot{\varphi}_{1,1} + \dot{u}_{N,1}) \cos \varphi_{1,1} + (x_i \dot{\varphi}_{1,2} + \dot{u}_{i,2}) \cos \varphi_{1,2}\}^T \quad (16)$$

The kinetic energy stored in a lumped mass on point  $A$  can be obtained then by

$$T_i = \frac{1}{2} m_i \vec{v}_A \cdot \vec{v}_A \quad (17)$$

That can be expanded to

$$T_i = \frac{1}{2} m_i \{ (l\dot{\varphi}_{1,1} + \dot{u}_{N,1})^2 + (x_i \dot{\varphi}_{1,2} + \dot{u}_{i,2})^2 + \\ 2(l\dot{\varphi}_{1,1} + \dot{u}_{N,1})(x_i \dot{\varphi}_{1,2} + \dot{u}_{i,2}) \cos(\varphi_{1,1} - \varphi_{1,2}) \} \quad (18)$$

The summation of the kinetic energies of all the elements yields the total kinetic energy of the second link as

$$T^{Link2} = \sum_{i=1}^N T_i \quad (19)$$

The overall kinetic energy of the linkage now can be arranged and rewritten as

$$T = T^{Link1} + T^{Link2} \equiv \frac{1}{2} \dot{\vec{q}}^T M \dot{\vec{q}} \quad (20)$$

That is a general way of describing the kinetic energy in a matrix form. The matrix  $M$  known as the global mass matrix of the system can be obtained by using equations, (12), (19), and (20).

The overall potential energy of the system does not depend on the velocity components and can be achieved by the summation of the strain energy of all elements under a deflection described by  $\vec{q}$  vector. The strain energy  $U^e$  stored in an Euler-Bernoulli beam element under small deflection  $u=u(x)$ ,  $-L/2 < x < L/2$  (Figure 2(a)) is given by the integral of the product of axial stress  $\sigma_x$  and strain  $\varepsilon_x$  over the volume of the element

$$U^e = \frac{1}{2} \int_V \sigma_x \varepsilon_x dv = \frac{1}{2} \int_{-L/2}^{+L/2} EI \left( \frac{\partial^2 u}{\partial x^2} \right)^2 dx \quad (21)$$

where  $I$  is the second moment of area of the cross-section;  $E$  is the elasticity modulus, and  $L$  is the length of the element. An approximate method to measure this integral is achieved using interpolation of the transverse displacement function  $u$  with Hermite shape functions. Defining the elemental coordinates vector  $\vec{X}_i^T = \{u_i, \varphi_i, u_{i+1}, \varphi_{i+1}\}^T$ , the potential energy of element “ $i$ ”, can be described in the following form

$$U_i^e = \frac{1}{2} \vec{X}_i^T K_e \vec{X}_i. \quad (22)$$

where the elemental stiffness matrix  $K_e$  is given by

$$K_e = \frac{EI}{L^3} \begin{bmatrix} 12 & 6L & -12 & 6L \\ 6L & 4L^2 & -6L & 2L^2 \\ -12 & -6L & 12 & -6L \\ 6L & 2L^2 & -6L & 4L^2 \end{bmatrix} \quad (23)$$

Through a proper transformation matrix  $\Gamma$ , the element coordinates vector  $\vec{X}$  can be related to the system coordinate vector  $\vec{q}$ , by

$$\vec{X} = \Gamma \vec{q} \quad (24)$$

Using (22) and (24) the overall potential energy can be obtained by a summation of the strain energies of all elements.

$$U = \sum U_i^e = \frac{1}{2} \sum \bar{X}_i^T K_e \bar{X}_i = \frac{1}{2} \bar{q}^T (\sum \Gamma^T K_e \Gamma) \bar{q} \equiv \frac{1}{2} \bar{q}^T K \bar{q} \quad (25)$$

The global stiffness matrix  $K$  is given by an assemblage algorithm provided by combining (23) and (25).

**B. Model Validation**

The linearized form of the governing equation of motion represented in (8) is given by

$$M \ddot{\bar{q}} + K \bar{q} = F \{\tau_1, \tau_2\}^T \quad (26)$$

Before applying the actual BCs, four measures were examined for checking the model; two numerical calculations, and two comparisons with commercial FE software Abaqus CAE. In the first two tests, the arm was supposed to be open (the links being in one line) and the generalized velocities were represented by imaginary vector fields so that a pure translational motion and a pure rotation are achieved. The conditions are shown in Figure 3.

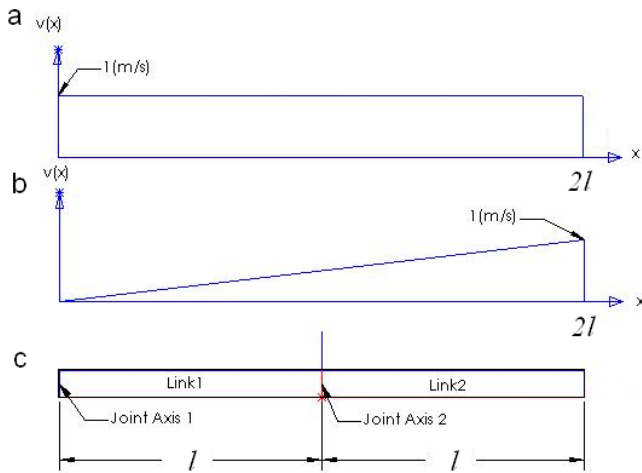


Fig.3 The assumptions for numerical tests: (a) velocity field for pure translation; (b) velocity field for rotation; (c) the open linkage.

In the first case, shown by Figure 3 (a),  $\dot{u}_{1,1} = 1, \dot{u}_{2,1} = 1, \dots, \dot{u}_{N,1} = 1$  and other velocity components are zero. Under such condition, all nodes would move by a velocity of 1m/s in the same direction, and therefore, the total kinetic energy of the system should be equal to the kinetic energy of a particle having a mass equal to the overall mass of the system, and moving with velocity 1 m/s. That was correct when numerically checked as follow

$$\frac{1}{2} \dot{\bar{q}}^T M \dot{\bar{q}} = \frac{1}{2} \sum_{i=1}^N M(i,i) \cdot (v(i))^2 \equiv \frac{1}{2} (m^{Link1} + m^{Link2}) * 1^2 = \frac{1}{2} (0.09450).$$

Note that this test cannot validate “all” the entries of  $M$  because rotational velocities are zero, and therefore the relevant components of  $M$  that are multiplied by the zero velocities will be vanished. For this reason in the second case shown by Figure 3 (b), a field of velocity was supposed so that the links rotate around the first joint by a constant unit angular velocity. This is achieved by putting

$$\dot{u}_{1,1} = 0, \dot{u}_{2,1} = l, \dot{u}_{3,1} = 2l, \dots, \dot{u}_{N,2} = (2N - 1)l$$

$$\dot{\phi}_{1,1} = \dot{\phi}_{2,1} = \dots = \dot{\phi}_{N,2} = 1$$

In this case, the kinetic energy must be equal to a rotating object having the total inertia of the links respect to joint “1” that is shown by  $(I_{link1/j1} + I_{link2/j1})$ , rotating with unit angular velocity. This condition was also satisfied according to the following relation

$$\frac{1}{2} \dot{\bar{q}}^T M \dot{\bar{q}} = \frac{1}{2} \sum_{i=1}^N M(i,i) \cdot (v(i))^2 \equiv \frac{1}{2} (I_{link1/j1} + I_{link2/j1}) * 1^2 = \frac{1}{2} (0.0248)$$

Additionally, the elastic deflections under such rigid body motions described by the two above mentioned cases will be zero and so it is expected that the overall potential energy be zero. For both of the motions the following test also was passed.

$$\frac{1}{2} \bar{q}^T K \bar{q} = \frac{1}{2} \sum_{i=1}^N \sum_{j=1}^N K(i,j) \cdot v(i) \cdot v(j) \approx 0$$

In the next two tests, the system is supposed to be supported to the ground so that the arm has not any rigid body motion. This is done by applying supporting BCs to (26). Two BCs, clamped-clamped-clamped (CCC) and clamped-clamped-free (CCF) were examined. In CCC, both joints as well as the tip of the arm are supposed to be clamped or welded to the ground, while in CCF the tip is free. The natural frequencies of the system given by the generalized eigenvalue problem is measured with “MATLAB”, and is compared to results of frequency analysis of the system using the Subspace Eigensolver of “Abaqus CAE”. The agreement between the results is shown in Table 2.

**C. The Transfer Matrix**

The next stage to complete the FE modeling procedure is exerting the BCs at the joints of the manipulator where the links are hinged to the ground and to each other. Applying the hinged BC means that for the first node of each link just rotational DOF are possible; that is

$$u_{1,1} = u_{1,2} = 0 \quad (27)$$

Applying (27) on (26) eliminates the 1<sup>st</sup> and  $(2N+1)$ <sup>st</sup> rows and columns from  $M$ ,  $K$ , and  $F$  to give the linearized equation of motion of the system as

$$\tilde{M}\ddot{\tilde{q}} + \tilde{K}\tilde{q} = \tilde{F}\{\tau_1, \tau_2\}^T \quad (28)$$

Then, a displacement/velocity state space representation of the linearized system can be represented as

$$\begin{aligned} \dot{X} &= AX + BV, \\ X &= \begin{Bmatrix} \tilde{q} \\ \dot{\tilde{q}} \end{Bmatrix}, A = \begin{bmatrix} O & I \\ -\tilde{M}^{-1}\tilde{K} & O \end{bmatrix}, B = \begin{bmatrix} O \\ \tilde{M}^{-1}\tilde{F} \end{bmatrix}, v = \begin{Bmatrix} \tau_1 \\ \tau_2 \end{Bmatrix} \end{aligned} \quad (29)$$

where  $O$  and  $I$  represent zero and identity matrices respectively. A Transfer Matrix (TM) of the system is achieved by selecting the proper output vector that includes the joint angles and displacement of the tip. The TM is represented by  $G$  as

$$\begin{Bmatrix} \varphi_{1,1} \\ \varphi_{1,2} \\ u_{N,2} \end{Bmatrix} = \begin{bmatrix} G_{11} & G_{12} \\ G_{21} & G_{22} \\ G_{31} & G_{32} \end{bmatrix} \begin{Bmatrix} \tau_1 \\ \tau_2 \end{Bmatrix} \quad (30)$$

The dashed line in (30) partitions  $G$  into six SISO systems  $G_{ij}$  representing the transfer function (TF) from input  $j$  to output  $i$ . The SISO system  $G_{31}$  (the TF from the first Input torque  $\tau_1$  to the third output  $u_{N,2}$  that is the displacement of the node at the tip of the manipulator) is expected to include all natural frequencies of the system. This is because when a force is applied at one physical end of a mechanical structure and measurement is performed at the other end, there would be no part outside these two ends that could cause hidden modes.

#### D. Convergence Analysis

The order of the system, which is determined by the size of the matrices in (28), depends on the number of elements that are used to discretize the links. By increasing the number of elements used in modeling a mechanical part, one may expect a more accurate model. However control engineers are more interested in low order systems, and so, have a tendency to discretize each link with low number of elements. For a high order system, not only designing a controller is difficult, but also numerical measurements for modeling and simulation such as matrix inversion and eigenvalue measurement tend to give more errors. On the other hand it is known that too low number of elements often cause loss of accuracy in FE Analysis. In the previous literature there is no analysis on choosing the necessary number of elements. In this study, the

number of elements is evaluated based on convergence of the time and frequency response of the FE model. The input output relation of the final FE model is required to be almost independent of the number of elements. In the following, it is shown that an FE model with low number of elements may not model dynamic behavior of a two-link FM precisely. Simulation of (28) can be performed using the Newmark integration method. A time simulation of the system with different number of elements is shown in Figure 4.

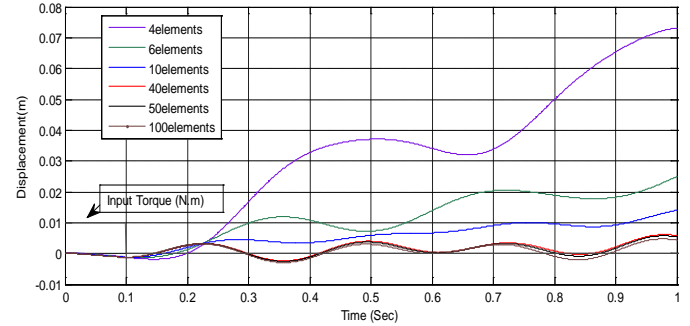


Fig.4 Time domain simulation of the FE model with 4,6,10,40,50, and 100 elements

A uniform pulse of magnitude 0.01 Nm and duration of 0.1 sec was applied on the  $G_{31}$  derived from the FE model in which each link is discretized to 4, 6, 10, 40, 50, and 100 elements. It can be seen that the output (the displacement of the tip) follows different trajectories depending on the number of elements. This dependence is more severe for lower number of elements. Figure 4 suggests that although both the gross motion and vibration behavior predicted by the FE model depends on the meshing resolution, but a convergence of the response is achieved with fine meshes. To investigate this fact, a frequency domain analysis is presented. The Frequency Response Function (FRF) of the FE model can be shown by Bode plots. Note that all of the FRF graphs in this paper show the “Receptance” that is the TF from force to displacement. Figure 5 shows the Bode magnitude plot of the  $G_{31}$  system with increasing the element number in a range between 2 to 10 elements for each link. It is observed in the graph that in this range the TF depends on the number of elements used for meshing the links. The predicted resonant frequencies of the system, that are represented by the frequencies of the peaks of the graph varies by increasing the elements. Even there is contradiction in prediction of the first natural frequencies that are crucial for controller design. A solution to resolve this problem can be given by using a finer mesh. The Bode plot of the models meshed with 20 to 70 elements is shown in Figure 6. The convergence of the curves implies that with a sufficient number of elements (around 50 elements), the FE model will not change severely with the number of elements. In other words, accurate input output characteristics of the system can be obtained by a FE model having any numbers of elements in the approximate range of 40 to 70. A finer mesh (more than 50 elements) does not influence the TF noticeably, but just increases the complexity of the system.

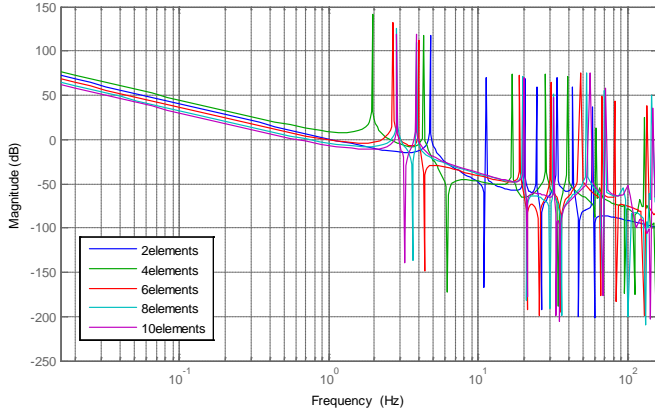


Fig.5 Inconsistency of the Bode plot of the FE model made up of low number of beam elements

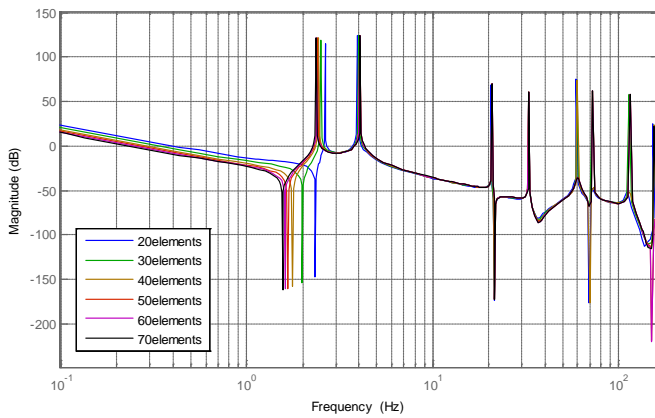


Fig.6 Convergence of the Bode plot of the FE model made up of 20 to 70 beam elements

On the other hand, by  $N-1$  elements ( $N$  nodes on each link), the mass and stiffness matrices  $M$  and  $K$  will be of order  $4N-2$ ; and so, increasing the elements may result in bigger errors in numerical calculations such as matrix inversion and eigenvalue measurement. Therefore it is decided that 50 elements are sufficient to model each link.

#### IV. THE MODAL MODEL OF THE SYSTEM

The state space model of the system with totally 100 elements has 202 states. However, generally, controller design algorithms have been developed for small to moderate size systems. Additionally, the high frequency vibrations that the high order FE model predicts, are not so important in practice, and are damped by the environment. To handle this problem, a model order reduction procedure is used to approximate the system to a lower order system, preserving low frequency characteristics of the system. For this reason, the system is broken into a set of second order systems using the modal decomposition technique. Then the reduced order model is recomposed of the most important components which in this work are considered to be the four-first vibration modes (modes within the bandwidth of 50 Hz) as well as two rigid body modes. The generalized eigenvalue problem is given by

$$\omega_n^2 \tilde{M} \tilde{Z}_n = \tilde{K} \tilde{Z}_n, \quad n=1,2,3,\dots,4N-2$$

$$\Lambda = [\tilde{Z}_1 \mid \tilde{Z}_2 \mid \tilde{Z}_3 \mid \dots \mid \tilde{Z}_{4N-2}] \quad (31)$$

Solving (31) yields  $n$  eigenvalues  $\omega_n^2$ , and  $n$  eigenvectors  $Z_n$ . Numerical measurements using MATLAB/LAPACK reveals  $n$  real natural frequencies shown here as  $\omega_1 \leq \omega_2 \leq \omega_3 \leq \dots \leq \omega_{4N-2}$ . The first natural frequencies of the system are given in Table 3. The system has two zero natural frequencies  $\omega_1 = \omega_2 = 0$  that represent the rigid body motion of the two-link manipulator. The matrix of eigenvectors is defined as the matrix containing the eigenvectors as its columns. For Modal Decomposition, a proper multiplication of the eigenvectors in (28) yields,

$$(\Lambda^T \tilde{M} \Lambda) \Lambda^{-1} \ddot{\bar{q}} + (\Lambda^T \tilde{K} \Lambda) \Lambda^{-1} \bar{q} = \Lambda^T \tilde{F} \{\tau_1, \tau_2\}^T \quad (32)$$

With a transformation represented by the eigenvector matrix, the mass and stiffness matrices are similar to block-diagonal matrices shown by  $\hat{M}, \hat{K}$  As

$$\hat{M} = \Lambda^T \tilde{M} \Lambda \quad \hat{K} = \Lambda^T \tilde{K} \Lambda$$

The parameters  $m_p$  and  $k_p$  do not have, necessarily, a physical meaning, and just show nonzero elements of the modal mass and stiffness matrices. With a change of variables, by defining modal coordinates, and modal input matrix  $\hat{f} = \Lambda^T \tilde{F} = [f_{i,j}]$ , (32) can be rewritten as

$$\hat{M} \ddot{\bar{z}} + \hat{K} \bar{z} = \hat{f} \{\tau_1, \tau_2\}^T \quad (33)$$

The first-two rows of (33) represent the “rigid body modes” of the system by

$$\begin{aligned} m_1 \ddot{z}_1 + m_{12} \ddot{z}_2 &= f_{1,1} \tau_1 + f_{1,2} \tau_2 \\ m_{21} \ddot{z}_1 + m_2 \ddot{z}_2 &= f_{2,1} \tau_1 + f_{2,2} \tau_2 \end{aligned} \quad (34a)$$

For  $p=3,4,\dots,4N-2$ , each row  $p$  of (33) is a decoupled equation representing one “vibration mode” of the system by

$$m_p \ddot{z}_p + k_p z_p = f_{p,1} \tau_1 + f_{p,2} \tau_2, \quad (34b)$$

Each vibration mode number “ $p$ ” has a resonant frequency  $\omega_p = \sqrt{k_p / m_p}$  that is identical to one of the natural frequencies of the original FE model. Beside showing the advantage of FE (over AMM which presumes the mode shapes), measuring the mode shapes helps to get better insight into the behavior of the system. Recalling  $\bar{z} = \Lambda^{-1} \bar{q}$ , the generalized coordinates are related to the modal coordinates

by  $\bar{q} = \Lambda \bar{z}$ , and the TF of  $G_{i,j}$  can be presented in terms of the summation of its modes

$$G_{i,j} = G_{i,j}^{Rigid} + \sum_{p=3}^{4N-2} \frac{\Omega_{i,p} f_{p,j}}{m_p s^2 + k_p}$$

$$\Omega_{i,p} = \begin{cases} \Lambda_{1,p} & i = 1 \\ \Lambda_{2N,p} & i = 2 \\ \Lambda_{4N-3,p} & i = 3 \end{cases} \quad (35)$$

Where the portion of rigid body modes given in (34a) is shown by  $G_{i,j}^{Rigid}$ . The FRF of  $G_{3,l}$  and the first modes of the FE model are shown in Figure 7. Near each natural frequency the system can be approximated by a single mode, while below the first natural frequency the system obeys a rigid body motion. This fact suggests that in replace for “all” the  $n$  modes in (35), the TF may be approximated by summation of “some” of the modes that have more important influence on the system (the modes that are within the bandwidth of interest are considered to be important). The solitary modes shown in Figure 8(a) are recomposed to form a reduced order system  $G_{i,j}^{Reduced}$  as

$$G_{i,j}^{Reduced} = G_{i,j}^{Rigid} + \sum_{p=3}^{NumMod} \frac{\Omega_{i,p} f_{p,j}}{m_p s^2 + k_p}$$

At this stage, to take into account the energy dissipation effects, a modal damping term  $2\zeta\sqrt{m_p k_p} s$  is added to the vibration modes to achieve

$$G_{i,j}^{Reduced} = G_{i,j}^{Rigid} + \sum_{p=3}^{NumMod} \frac{\Omega_{i,p} f_{p,j}}{m_p s^2 + 2\zeta\sqrt{m_p k_p} s + k_p} \quad (36)$$

High frequencies (here higher than 50 Hz) are not of interest, and so the fifth and higher vibration modes can be truncated from (36). By choosing  $NumMod=6$  the superposition is done up to 6 modes including the two rigid body modes as well as the four vibration modes in the bandwidth. Figure 8 shows the FRF plots of the original FE model and the reduced order system.

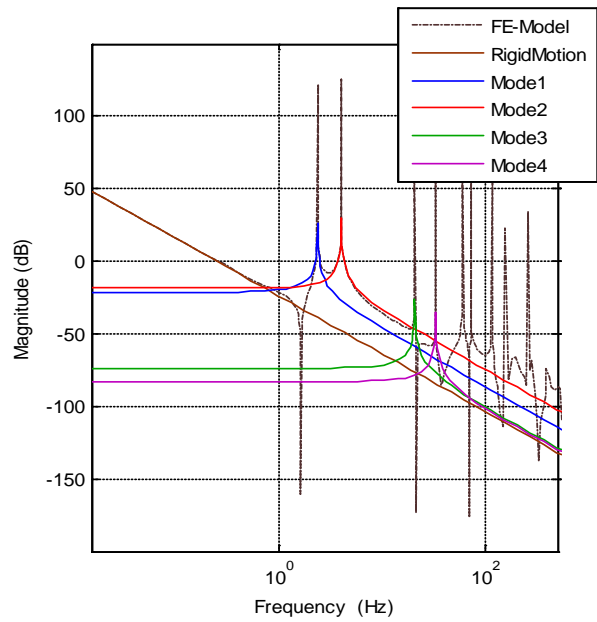


Fig.7 The FE model and the first modes.

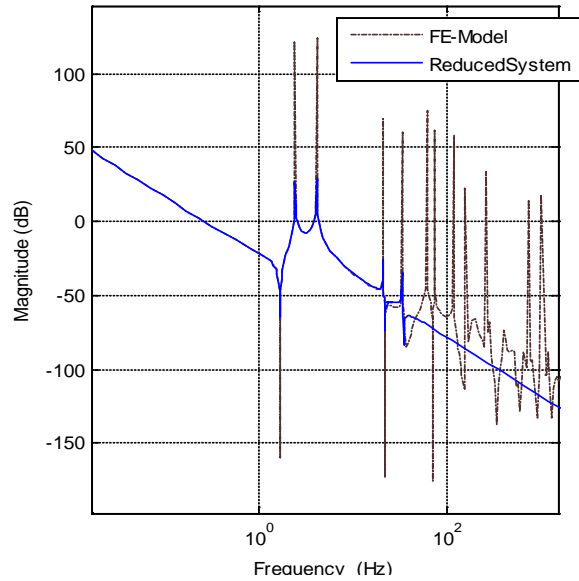


Fig.8 The FE model and the reduced system.

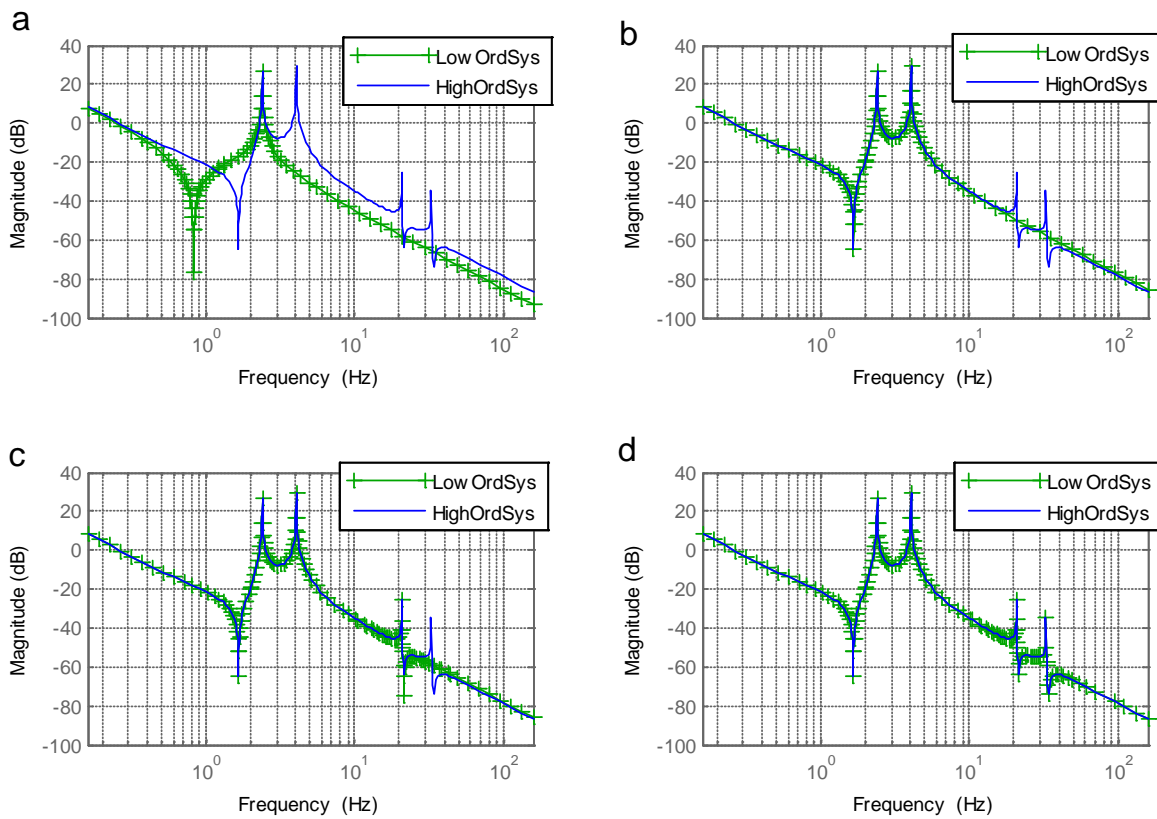


Fig.9 Comparison of the high order system (HighOrdSys) with the reduced order models (LowOrdSys) having: (a) one, (b) two, (c) three, and (d) four vibration modes

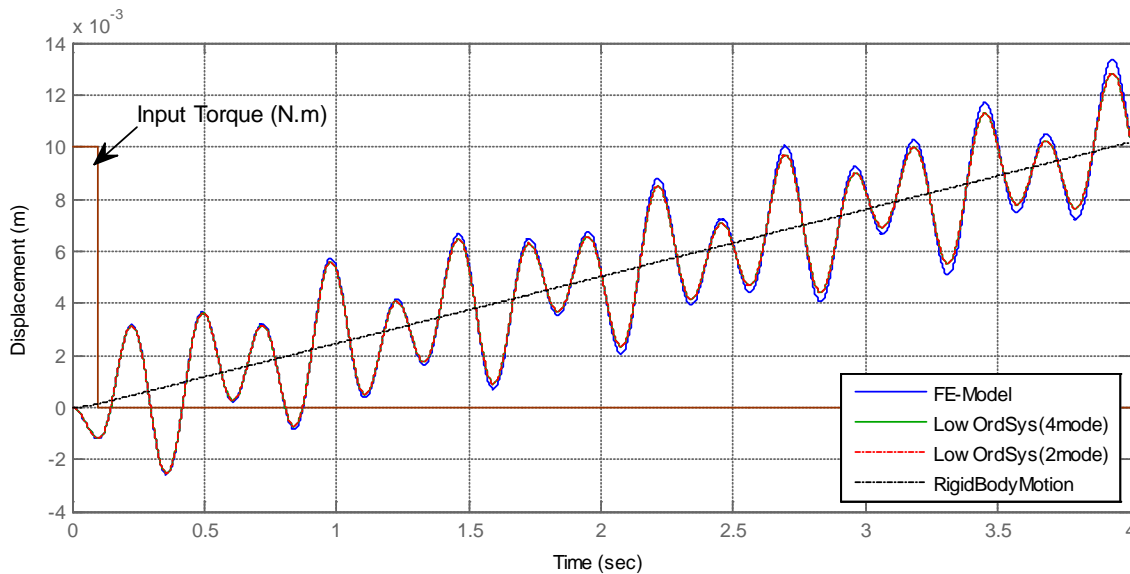


Fig.10 Displacement of the tip of the manipulator measured with the FE model and the Reduced Systems

At low frequencies the plots agree perfectly. At resonances the amplitudes of the FE model becomes theoretically very high, but it cannot be realistic because even when all viscous effects are zero, the material of the links has a structural damping that can be modeled by a small  $\zeta$ , that here is supposed to be  $\zeta = 0.002$

The procedure to select the required order of reduction is

shown in Figure 9 in which the Bode plot of the high order system is compared with the reduced systems having one (Figure 9 (a)), two (Figure 9 (b)), three (Figure 9 (c)), and four vibration modes (Figure 9 (d)). As more vibration modes are included, the model becomes more precise and predicts more resonances. It is inferred that considering four vibration modes is necessary and sufficient to include four resonant frequencies and approximate the model in the control bandwidth. However

Figure 9 (b) suggests that the model with two vibration modes may be sufficient to model the dynamics of the system for controller design, though it cannot predict two higher resonances that are yet in the bandwidth of interest. In fact the amplitude or the  $H_\infty$  norm of the third and the fourth vibration modes are very small compared with the first and the second modes, and according to  $H_\infty$  model reduction technique, can be eliminated from the model.

In order to observe the ability of the reduced models in modeling the behavior of the FE model in time domain, an input torque of amplitude 0.01 Nm and duration of 0.1 sec was applied on the FE model and the reduced systems. The result of the simulation is shown in Figure 10 which shows the response of the FE model and the reduced systems having two and four vibration modes. It can be seen that the output of the reduced models matches with that of the original FE model. Recalling that the reduced system includes modal damping, the decay in the amplitude as proceed in time is expectable. The straight line in Figure 10 shows the rigid body motion of the tip. The presented comparisons, in time and frequency domains, show that the reduced order systems are able to model the input-output behavior of the FE model.

## V. CONCLUSION

A high resolution FE model was developed for modeling a two-link flexible manipulator that can reveal the global vibration modes of the system. It was shown that modeling the system with low number of elements may not satisfy convergence conditions of the dynamic problem. In order to use the model in controller design algorithms, in contrast with the previous custom in literature that is constructing the FE model with low number of elements, the high order model was approximated to a low order system using modal truncation/ $H_\infty$  technique.

## REFERENCES

- [1] S. B. Skaar and C. F. Ruoff, *Teleoperation and Robotics in Space*: American Institute of Aeronautics and Astronautics, Inc., 1994.
- [2] W. J. Book, O. Maizza-Neto, and D. E. Whitney, "Feedback Control of Two Beam, Two Joint Systems with Distributed Flexibility," *Journal of Dynamic Systems, Measurement, and Control*, vol. 97, pp. 424-431, 1975.
- [3] S. Yu and M. A. Elbestawi, "Modelling and Dynamic Analysis of a Two-Link Manipulator with both Joint and Link Flexibilities," *Journal of Sound and Vibration*, vol. 179, pp. 839-854, 1995.
- [4] P. B. Usoro, R. Nadira, and S. S. Mahil, "A Finite Element/Lagrange Approach to Modeling Lightweight Flexible Manipulators," *Journal of Dynamic Systems, Measurement, and Control*, vol. 108, pp. 198-205, 1986.
- [5] J. D. Lee and W. Ben-Li, "Dynamic Equations for a Two-Link Flexible Robot Arm," *Computers and Structures*, vol. 29, pp. 469-477, 1988.
- [6] J. M. Martins, Z. Mohamed, M. O. Tokhi, J. Sa da Costa, and M. A. Botto, "Approaches for Dynamic Modelling of Flexible Manipulator Systems," *IEE Proceedings of Control Theory and Applications*, vol. 150, pp. 401-411, 2003..
- [7] M. Sayahkarajy and Z. Mohamed, "Mixed sensitivity  $H_2/H_\infty$  control of a flexible-link robotic arm," *International Journal of Mechanical & Mechatronics Engineering*, vol. 14, 2014.
- [8] M. Sayahkarajy, Z. Mohamed, A. A. M. Faudzi, and E. Supriyanto, "Hybrid vibration and rest-to-rest control of a two-link flexible robotic

arm using  $H_\infty$  loop-shaping control design," *Engineering Computations*, vol. 33, 2016

- [9] J. U. Duncombe, "Infrared navigation—Part I: An assessment of feasibility (Periodical style)," *IEEE Trans. Electron Devices*, vol. ED-11, pp. 34–39, Jan. 1959.